

# 7T vs. 4T: RF Power, Homogeneity, and Signal-to-Noise Comparison in Head Images

J.T. Vaughan,<sup>1\*</sup> M. Garwood,<sup>1</sup> C.M. Collins,<sup>2</sup> W. Liu,<sup>2</sup> L. DelaBarre,<sup>1</sup> G. Adriany,<sup>1</sup> P. Andersen,<sup>1</sup> H. Merkle,<sup>1</sup> R. Goebel,<sup>3</sup> M.B. Smith,<sup>2</sup> and K. Ugurbil<sup>1</sup>

**Signal-to-noise ratio (SNR), RF field ( $B_1$ ), and RF power requirement for human head imaging were examined at 7T and 4T magnetic field strengths. The variation in  $B_1$  magnitude was nearly twofold higher at 7T than at 4T (~42% compared to ~23%). The power required for a 90° pulse in the center of the head at 7T was approximately twice that at 4T. The SNR averaged over the brain was at least 1.6 times higher at 7T compared to 4T. These experimental results were consistent with calculations performed using a human head model and Maxwell's equations. *Magn Reson Med* 46:24–30, 2001. © 2001 Wiley-Liss, Inc.**

**Key words:** high-field MRI; RF power; RF homogeneity; signal-to-noise

In the last decade, MRI studies conducted at 4T have demonstrated the utility of high magnetic fields in functional and anatomical imaging of the human brain and for spectroscopy studies in the brain and the human body (1–7). These accomplishments and the continued successes at magnetic fields up to 9.4T with animal models have paved the way for the exploration of magnetic fields of higher than 4T for human brain studies (8–12). Consequently, recent efforts have been undertaken to establish 8T and 7T systems, the latter in our laboratory (13–15). Now with an operational 7T system, the signal-to-noise ratio (SNR), RF field ( $B_1$ ), and RF power requirement at 7T were compared to the same parameters at 4T.

## MATERIALS AND METHODS

In this 7T vs. 4T comparison study, we used the same size coils, the same model consoles, identical acquisition parameters, and the same volunteers for six carefully reproduced experiments at each field strength.

### Hardware

#### Systems

This experiment was performed on Varian Unity Inova consoles interfaced to 90 cm bore Oxford 4T and Magnex 7T magnets. The noise figures of the two systems were the

same, measuring 1.3 dB. Siemens body gradients (65 cm i.d.) and Magnex head gradients (38 cm i.d.) were used in the 4T and 7T systems, respectively.

#### Coils

Two 16-element TEM head coils of the same dimensions (Fig. 1a) were built and tuned to 300 MHz and 170 MHz, respectively (16–18). The coils measured 27 cm in diameter at the element centers. The TEM cavity (coil length) measured 17 cm from the back closed wall to the front open wall (head entry side). The use of a back wall in the TEM cavity allows for a shorter, more efficient, and better shielded coil. Each coil was driven in quadrature at four points, 45°, 135°, 225°, 315°, relative to 0° at the bottom of the coil (16,18). Consistent with the literature (16,18,19), the 300 MHz coil had an unloaded Q to loaded Q ratio of 432/66 and the 170 MHz coil's Q ratio was 850/78. The  $B_1$  gain, defined as the ratio of coil  $B_1$  field strength to coil input signal, was 1 dB less at volume center for the 300 MHz coil compared to the 170 MHz coil. This gain measurement provides a direct bench determination of the  $B_1$  field generation efficiency of a coil for a reference sample space. Both coils and the dipole field probe were matched to 50Ω at the network analyzer used for this measurement. While a 1 dB difference in gain between the two coils was noted and considered in the conclusion of this comparison study, the data presented in this report are practical and do not calibrate for 1 dB coil loss (to radiation resistance) at 300 MHz.

$B_1$  homogeneity over a 14 cm brain sized diametric cylindrical volume (dcv) for both coils was verified by bench measurement and by NMR methods to vary by less than 1 dB. In the NMR experiment, five 1.5 × 10 cm centrifuge tubes were filled with mineral oil and coaxially positioned in the center of the coil, in the pattern shown in Fig. 1b,c. The sparsely spaced mineral oil-filled tubes presented no conductive loading. Their electrical length was approximately 1/7 λ at 300 MHz. Therefore, load and resonance effects from this sparse tube phantom were negligible and did not perturb the homogeneity measurement of the essentially unloaded coil. The profiles of the imaged sparse tube phantoms show signal intensity variation of well under 10% over the centered 14 cm dcv beginning at the back wall of the coil (Fig. 1b,c). Both coils were homogeneous.

#### Model

Full-wave  $B_1$  field profile predictions were numerically calculated by the Finite Difference Time Domain (FDTD) method at 4T and 7T (20). This widely used method for calculating electromagnetic fields was implemented on a

<sup>1</sup>Center for MR Research, Department of Radiology, School of Medicine, University of Minnesota, Minneapolis, Minnesota.

<sup>2</sup>Center for NMR Research, Department of Radiology, Pennsylvania State University College of Medicine, Hershey, Pennsylvania.

<sup>3</sup>Brain Innovation B.V. Postbus 1142, 6201 BC Maastricht, The Netherlands.

Grant sponsor: NIH; Grant numbers: CA76535; CA64338; RR08079; Grant sponsors: W.M. Keck Foundation; National Foundation for Functional Brain Imaging; Whittaker Foundation.

\*Correspondence to: J. Thomas Vaughan, Ph.D., Center for Magnetic Resonance Research, 2021 Sixth Street S.E., Minneapolis, MN 55455. E-mail: tommy@cmrr.umn.edu

Received 2 June 2000; revised 2 February 2001; accepted 2 April 2001.

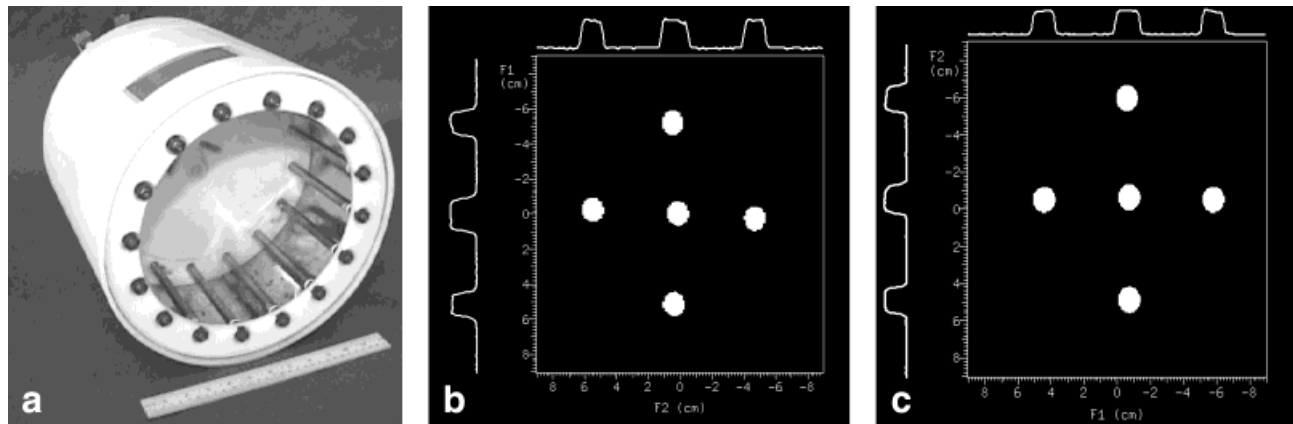


FIG. 1. The TEM head coil used (a) was verified to be homogeneous at 7T (b) and at 4T (c). The images (b,c) are transaxial slices through  $1.5 \times 10$  cm oil-filled tubes centered in the TEM coil. Their profiles show equal intensity across the FOV of the coil in the x-y plane.

rectilinear grid having a resolution of 5 mm in each dimension. The predictions were derived from a 3D model incorporating the National Library of Medicine (NLM) Visual Human Project's digitized male head within a model of a 16-element TEM resonator having the same dimensions as those used in the experiments, but open on both ends. The TEM resonator was tuned to the desired frequency (170 or 300 MHz) while containing the head model with appropriate electrical properties at each frequency (21) by using a Gaussian excitation and a Fourier transform of the time domain response (20). Tuning was performed by lengthening or shortening the inner conductors of the elements in the TEM model as needed (as in experiment). After the coil model was tuned it was excited with one-volt potentials across the same four capacitive gap locations as in the experimental coils (16,18). Then the magnitudes of the positive ( $B_1^+$ ) and negative ( $B_1^-$ ) circularly polarized magnetic field components were calculated (22) for counterclockwise and clockwise drives, respectively. An intrinsic SNR (ISNR) was then calculated (23,24):

$$ISNR \propto B_0^2 \frac{|\sin(VB_1^+ \gamma \tau)| B_1^-}{\sqrt{P_{abs}}}$$

where  $B_0$  is the magnitude of the static field,  $V$  is a dimensionless normalization factor proportional to coil driving voltage,  $\gamma$  is the gyromagnetic ratio,  $\tau$  is the duration of the  $B_1$  pulse, and  $P_{abs}$  is the absorbed power during the unit-voltage  $B_1$  pulse. This definition of ISNR does not consider power lost to radiation from the coil. The value for  $V$  is that resulting in a  $90^\circ$  flip angle ( $VB_1^+ \gamma \tau$ ) at the center of the head after a  $\tau = 3$  ms rectangular pulse. Values for  $B_1^+$ ,  $B_1^-$ , and  $P_{abs}$  are those corresponding to unit driving voltages in the coil.

#### Measurements

Six comparison studies were performed by imaging each of the volunteers at both field strengths. Four healthy normal adults volunteered, two were imaged twice and two were imaged once each for the six-experiment study. The pool of volunteers included an Asian female, an Asian-Caucasian male, an African male, and a Caucasian

male. All heads were positioned in the coils to the same depth, such that the top of the head rested against a 1 cm spacer from the back wall of the coil. Evidence of this positioning and a full-length head field of view (FOV) can be observed in the sagittal spin echo images (Fig. 2). Sagittal scout images were used to locate a transaxial image slice through the center of the brain for this investigation. Slices that avoid the central portion of the brain can yield more uniform images and  $B_1$  profiles. For example, non-center slice 7T images appear more uniform in Fig. 6 than

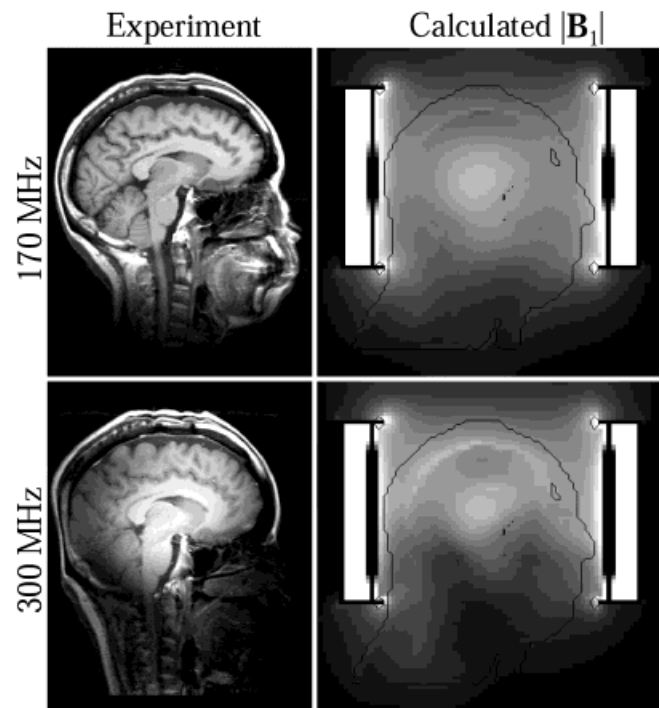


FIG. 2. Multislice spin-echo MDEFT images were acquired at 4T (top) and at 7T from the same head and position with equal-sized coils and the same image parameters. Note the inhomogeneity at 7T compared to 4T. Full-wave  $B_1$  field profile predictions (right) were numerically calculated by the Finite Difference Time Domain (FDTD) method at 4T (top) and 7T.

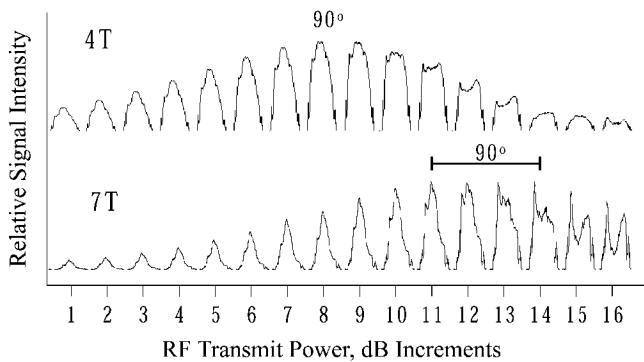


FIG. 3. To determine RF power calibrations at 4T (top) and 7T (bottom), one-dimensional projections across the head (anterior-posterior direction) were acquired and plotted as a function of RF power. The RF power setting (dB) that produced a maximum signal anywhere in the projection was chosen to represent the best average  $90^\circ$  flip angle, assuming negligible  $T_2^*$  dephasing during the short TE (5 ms) used. At 4T, the  $90^\circ$  pulse was reached for most of the head approximately simultaneously. At 7T, the  $90^\circ$  power requirement was more highly dependent on nonuniform  $B_1$  contours over the head.

do slices through the center of the brain. However, for this study a transverse slice through the brain center was chosen for evaluation of the *inhomogeneities* in the human brain at 7T and at 4T. The RF power calibration,  $B_1$  homogeneity, and SNR were measured over this transaxial center slice in each of the volunteers at each field strength.

#### Calibration of RF Source

The RF power was calibrated in order to determine the RF power setting to be employed during image acquisition for the SNR comparison and  $B_1$  field mapping. The RF power was calibrated using a projection of the transaxial slice signal intensity (Fig. 3). No phase-encode gradient was used. These measurements were performed with a spin-echo sequence in which the voltage of the second (refocusing) pulse was set to twice the first (excitation) pulse. The RF power of these pulses was simultaneously incremented by 1 dB steps. As the power was incremented, full recovery of the longitudinal magnetization ( $TR = 10$  s) was allowed between consecutive acquisitions. Identical acquisition parameters were used at both fields.

While the above method for calibrating RF power from image signal intensity projections is standard and convenient, the RF power calibration for a local region in the head is more accurately determined from the  $B_1$  measurement from that region, as described below.

#### $B_1$ Field Distribution

The  $B_1$  distribution over the head was mapped using magnetization-prepared ultrafast gradient echo (turboFLASH) (25). Magnetization preparation was accomplished with a variable-duration hard (square) pulse followed by rapid gradient spoiling to eliminate transverse magnetization. The resultant longitudinal magnetization was imaged rapidly using turboFLASH (center-out  $k$ -space sampling,  $TR/TE = 4.2/2.5$  ms, slice thickness = 5 mm, flip angle =  $10^\circ$

at the slice center, matrix size =  $128 \times 64$ ). A total of 21 such images were acquired each with a different duration of the magnetization preparation pulse which was incremented from 0–2 ms in 100  $\mu$ s steps. Full relaxation was allowed between consecutive images. The power for the magnetization preparation pulse was set sufficiently high to minimize off-resonance effects (870 W and 644 W for 4T and 7T, respectively). The signal intensity modulation as a function of the preparation pulse duration at each pixel in the image directly measured the  $B_1$  magnitude in frequency units at that location (Fig. 4).

#### Signal-to-Noise Ratio

For comparing the SNR, density-weighted gradient-echo images were acquired using the parameters:  $TR/TE = 5000/5$  ms,  $NEX = 1$ , receiver bandwidth = 100 kHz, slice thickness = 5 mm with a 2 ms Gauss-shaped pulse,  $FOV = 24 \times 22$  cm, matrix size =  $256 \times 256$ . The RF power used to produce a  $90^\circ$  flip angle at the slice center was determined by the RF pulse calibration method described above. The same receiver bandwidth was used for both the 7T and 4T studies. These acquisition parameters were used for all six studies at both fields. The SNR was determined from these fully relaxed images by dividing the mean pixel value within an image ROI by the mean pixel value of artifact-free background. The SNR measurements were sampled from the white matter ROIs in the same five positions (left and right parietal, frontal, occipital, and center) on each of the six images at each field and then averaged (Fig. 7).

#### Spin-Echo Images

Multislice spin-echo images provided a qualitative comparison of human head imaging at 7T and 4T. The multislice spin-echo MDEFT sequence (1,26) was used to acquire  $T_1$ -weighted anatomical images with the parameters:  $TR/TE/TI = 1500/13.5/750$  ms,  $NEX = 2$ , receiver bandwidth = 48 kHz, four slices,  $thk = 3.5$  mm with 4.5 ms 3-lobe sinc-shaped pulses for excitation and refocusing, 78 ms frequency-swept (chirp) inversion, sagittal  $FOV = 30 \times 24$  cm, axial  $FOV = 24 \times 22$  cm, and matrix size =  $256 \times 256$ . This sequence was used to acquire the images in Figs. 2 and 6.

#### Intensity Correction

Signal intensity variation in high-field images can be corrected when “uniform” images are desired. An algorithm by BrainVoyager (Brain Innovation, Maastricht, The Netherlands) was used to achieve apparent image homogeneity in 7T images (Fig. 8). The intensity inhomogeneity correction algorithm estimated a 3D bias field by fitting Legendre polynomials to presegmented tissue data. A crude initial segmentation of white matter was sufficient to estimate the nonuniformity and to extrapolate this estimation to the rest of the brain. Better accuracy could be achieved through iteration.

## RESULTS AND DISCUSSION

### RF Power Requirement

The RF power requirement for each head image was determined from the power needed to obtain the first maxi-

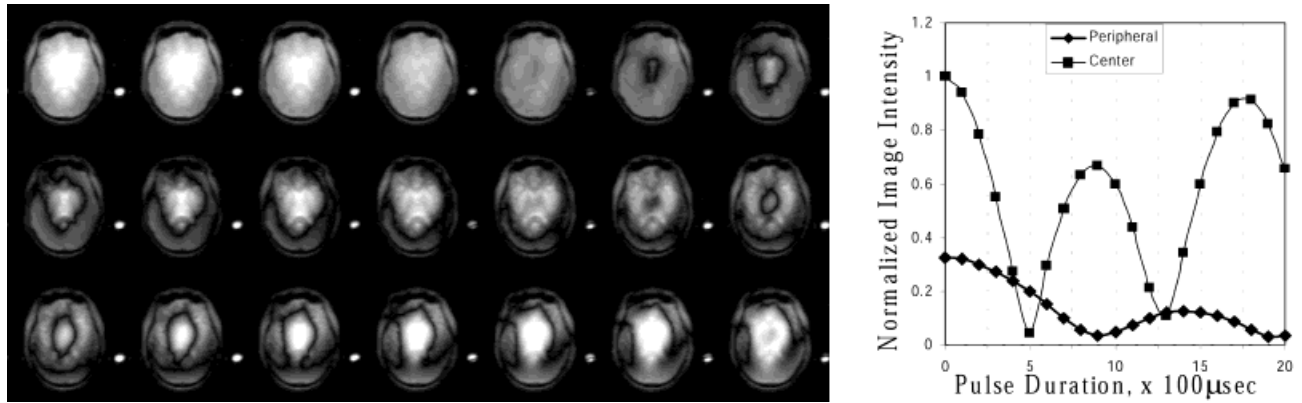


FIG. 4. The  $B_1$  distribution over the head was mapped with 21 turboFLASH images corresponding to preparation pulse lengths from 0–20 ms in 100  $\mu$ s steps (left). The 21 images acquired at 7T reveal the spatial dependence of the  $M_z$  modulation induced by the incremented preparation pulse. The central and peripheral signal intensities were plotted for each of the 21 images (right). The difference in intensity oscillations between the two curves provides a measure of difference in  $B_1$  (inhomogeneity) between the center and the periphery of the brain. 4T,  $B_1$  measurements were similarly acquired.

imum MR signal intensity in the spin-echo calibration sequence as RF power amplitude was incremented in 1 dB steps (Fig. 3). The calibrated  $90^\circ$  flip angles in the center of the brain were 255  $\mu$ sec and 369  $\mu$ sec at 4T and 7T, respectively, for a 1 kW equivalent square pulse averaged over six studies. The calibrated  $90^\circ$  pulse for 4T compared well with previously reported values (16,19). Thus, 2.1 times more power was needed at 7T compared to 4T to attain  $90^\circ$  in the *center* of the brain. In the Maxwell model, the power absorbed by the head model to achieve the same  $B_1^+$  magnitude at the center of the head model is 1.8 times greater at 7T than at 4T. This calculated value is in good agreement with the experiment, especially when the 7T coil is compensated for its 1 dB relative gain loss to radiation, in which case the 7T/4T power requirement is 1.9. The power required to achieve a  $90^\circ$  rotation is spatially nonuniform over the brain at 7T, and is least at the center, where the  $90^\circ$  rotation occurs first (Figs. 2, 5, 6). In the brain periphery approximately 3 dB additional power is required to reach  $90^\circ$  compared to the brain center. This strong spatial dependence of the flip angle on RF power is evidence of a nonuniform  $B_1$  field across the human head at 7T.

#### $B_1$ Field (In)homogeneity

To measure and compare the  $B_1$  field contours, the  $B_1$  field was mapped across transaxial slices at 7T and at 4T (Fig. 4). The series of 21 images with incremented RF pulse durations shows the familiar “bull’s eye” intensity pattern seen in high-field phantom images (16,27,28). In these images the resultant longitudinal magnetization following a variable-duration square pulse is mapped. Therefore, the image intensity of these magnitude images is directly proportional to the absolute value of  $\sin \theta$ , where  $\theta$  is equal to  $\gamma B_1 \tau$  ( $\tau$  is the duration of the magnetization preparation pulse). As  $\tau$  is incremented over a period that exceeds  $(\gamma B_1)^{-1}$  the signal intensity oscillates with the frequency  $\gamma B_1$ . It should be noted that while the signal amplitude over the image will be affected by variations in both  $B_1$  magnitude and  $T_1$  relaxation effects in the turboFLASH

image acquisition, the *frequency* of signal oscillation will be a function of  $B_1$  only. With a relative permittivity of approximately 55 at 300 MHz, the brain supports a propagating wave  $\lambda$  of 12 cm (21). Constructive wave superposition crests in the brain center. Therefore, signal intensity oscillates with higher frequency in the brain center than in the periphery. This oscillation is plotted for the center and peripheral regions of the brain image in Fig. 4b. The first

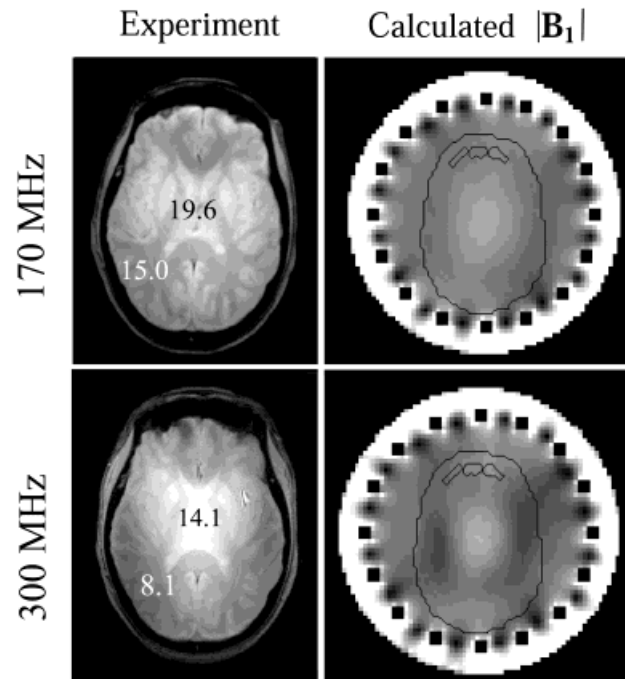


FIG. 5. In these gradient echo images the  $B_1$  homogeneity of 4T (top) was compared to 7T (bottom) for a homogeneous TEM head coil. Averaged  $B_1$ ,  $\mu$ T values standardized to a 1 kW RF excitation pulse equivalent are shown on representative head images from the central and peripheral regions from which they were measured. Maxwell  $B_1$  field profile predictions (right) were numerically calculated for 4T (top) and for 7T.

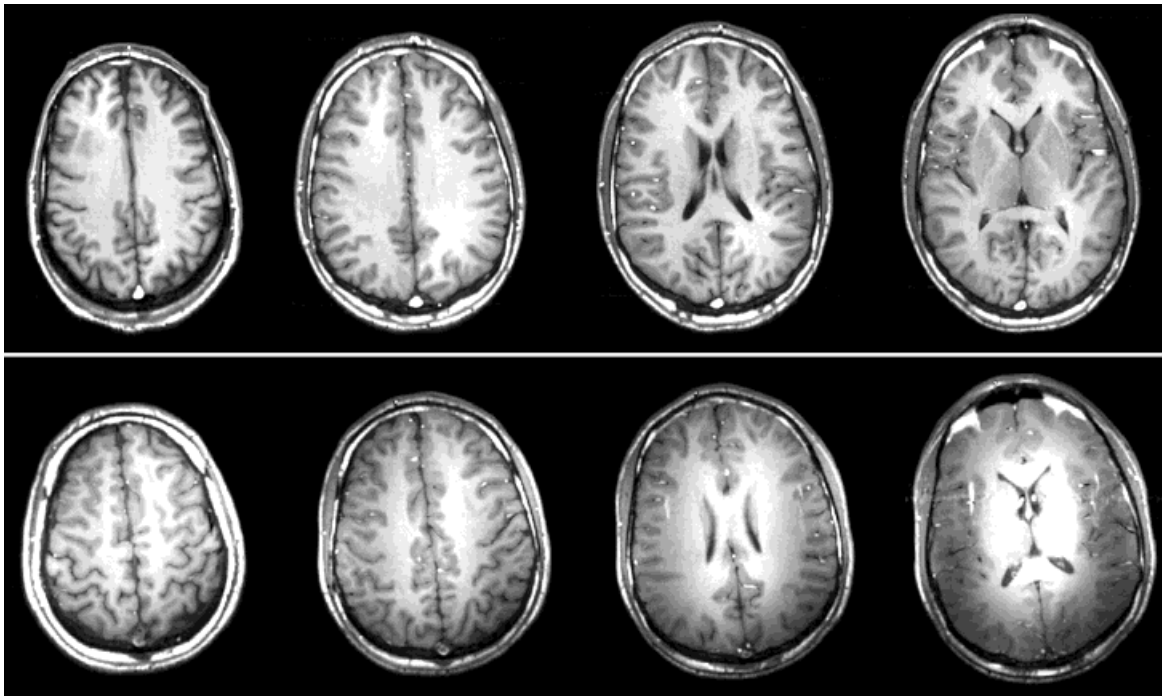


FIG. 6. MDEFT spin-echo head images at 4T (top) and at 7T (bottom) were acquired using the same parameters. The relative increase in  $B_1$ -dependent inhomogeneity of the 7T images is obvious, especially for the deep brain.

null in these plots corresponds to where the flip angle  $\theta = 90^\circ$ . Averaged  $B_1$  values for  $\theta = 90^\circ$  in the brain center were adjusted to their 1 kW RF pulse equivalents and depicted on their respective comparison slices for 4T and 7T (Fig. 5). At 4T the  $B_1$  strength in the brain periphery is down 23.5% from the center value. At 7T the peripheral  $B_1$  is 42.5% lower than the central  $B_1$ . Based on the  $B_1$  gradient from the center to the parietal edge of the brain, the 7T

image is, on average, 19% less homogeneous than the 4T images studied.

Compared to 4T, the lower  $B_1$  values in the 7T image for a 1 kW pulse indicate the additional power required for imaging the head at 7T. Calculating power from these experimental  $B_1$  values, 1.9 times more power was required to achieve a  $90^\circ$  flip angle in the center of the head at 7T compared to 4T. Calibrating for the 1 dB coil differ-

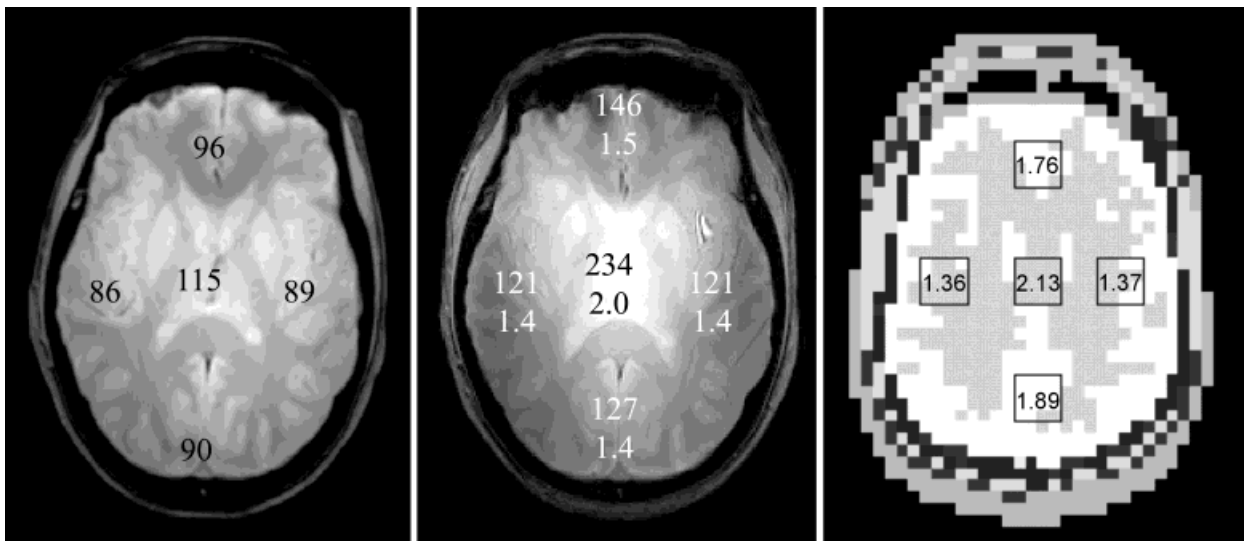


FIG. 7. The SNR was measured from fully relaxed gradient echo images acquired using the same acquisition parameters and homogeneous TEM volume coils at 4T (left) and at 7T (center). Averaged, regional SNR measurements are shown on the images. Average 7T/4T SNR ratios are listed beneath the SNR data on the 7T image. A Maxwell model (right) with calculated 7T/4T SNR values compares favorably.

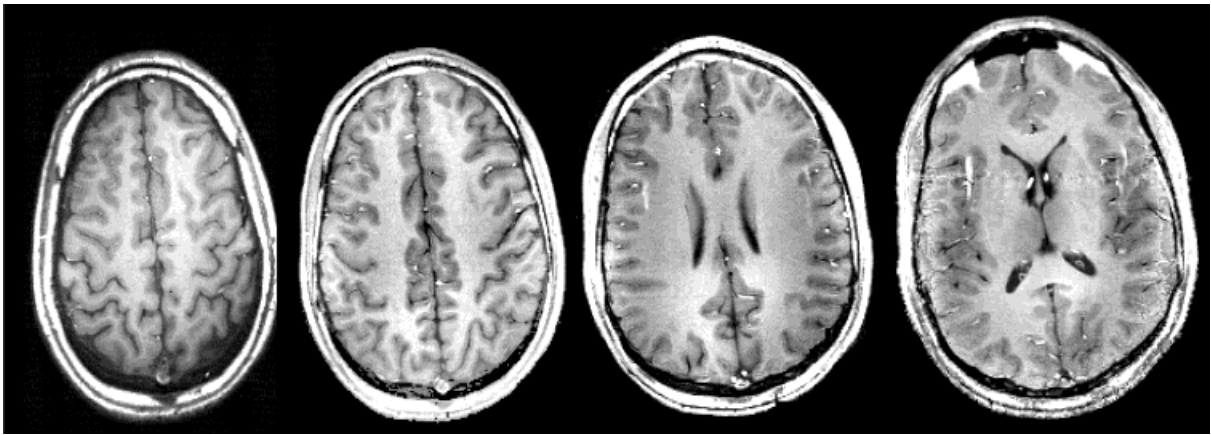


FIG. 8. The MDEFT spin-echo 7T images from Fig. 6 were intensity-corrected to give apparent homogeneity in images with improved 7T signal-to-noise.

ence again, the power factor between 4T and 7T rounds to 1.8. This value was in excellent agreement with the image signal intensity measurement of 1.9 calibrated (Fig. 3) and the theoretical model prediction of 1.8. As above, a factor of 2.0 times (3 dB) additional power was required to reach a  $90^\circ$  flip angle in the periphery of the head. The nonuniform  $B_1$  profiles and dependent power requirements obtained experimentally were both expected and accurately predicted by Maxwell models of the head-loaded TEM coil (Fig. 5).

The inhomogeneity revealed in the  $B_1$  maps is clearly evident in spin-echo images of the brain at 7T (Fig. 6). While slices distant from the center of the brain can be more homogeneous, a large signal intensity variation becomes obvious in slices through the center of the brain.

#### Signal-to-Noise

SNR measurements were taken from pairs of  $7 \text{ mm}^2 \times 5 \text{ mm}$  voxels in each of the five positions shown on the representative density-weighted gradient echo images (Fig. 7). An effort was made to sample the same tissue (white matter) in each of these positions. The numbers shown are averages for the six studies. While the SNR measurements reveal the expected  $B_1$  spatial dependence at both field strengths, the SNR at 7T is increased over the whole slice compared to 4T. For comparison the 7T/4T, SNR ratios are shown beneath the averaged SNR data on the 7T image. Averaging the five experimental 7T/4T ratios, the 7T image has 1.6 times the SNR of the 4T image. When the 300 MHz coil is calibrated by 1 dB to match the  $B_1$  gain of the 170 MHz coil, the 7T SNR is 1.76 times the 4T value. Thus, the linear trend in SNR improvement observed for head imaging at fields from 1.5T to 3T to 4T continues to hold for 7T. The predicted 7T/4T SNR ratios are shown on the Maxwell model of the same head slice at 7T, in good agreement with the experimental results. Values in anterior and posterior regions of the brain model are a little higher than those in the experiment. This result might be attributed to the differences in head geometry between the model and an “average” head. The average of the calculated ratios in the five regions of the model is

1.7 compared to the experimental value of 1.6, calibrated to 1.76.

The ratios shown in Fig. 7 reflect the SNR obtained when the center of the brain experiences a  $90^\circ$  pulse while the periphery undergoes a less than  $90^\circ$  rotation. The SNR values for 7T and 4T would be higher at the periphery if a uniform  $90^\circ$  excitation, as is possible with an adiabatic pulse, were attained. An adiabatic sequence approach to uniform excitation, however, does not imply uniform reception. Alternatively, the  $B_1$  profile of an RF coil might be biased to effect a more uniform excitation and reception in the human head.

Given the improvement in SNR, image homogeneity at 7T may not be necessary or desirable for many applications.  $B_1$  field profiling with surface coils for superficial regions of interest, or with volume coils for deep brain regions, may find great advantage in 7T biomedical applications. Where homogeneous images are desired, however, intensity correction in image postprocessing provides a simple means to a homogeneous image with improved 7T SNR (Fig. 8).

#### CONCLUSIONS

For a transaxial slice through the center of the head, the following conclusions are reported. In a homogeneous head coil, the RF power required for a  $90^\circ$  pulse to the center of the head at 7T is approximately twice that of 4T. For the same homogeneous head coil and transverse slice, the  $B_1$  inhomogeneity at 4T is 23% compared to 42% at 7T. Most importantly, the averaged SNR at 7T is at least 1.6 times that of 4T. The RF power requirements, the RF homogeneity, and the signal-to-noise are all dependent on the nonuniform  $B_1$  field contours over the head at 7T and at 4T. These findings are in agreement with predictions using current MR theory and Maxwell calculations of the RF fields at these frequencies.

#### ACKNOWLEDGMENTS

The authors thank Drs. Seong-Gi Kim, Xiaoping Hu, Wei Chen, Rolf Gruetter, and the staff and students of the

University of Minnesota's Center for Magnetic Resonance Research.

## REFERENCES

- Ugurbil K, Garwood M, Ellermann J, Hendrich K, Hinke R, Hu X, Kim S-G, Menon R, Merkle H, Ogawa S. Imaging at high magnetic fields: initial experiences at 4T. *Magn Reson Q* 1993;9:259–277.
- Ugurbil K, Hu X, Chen W, Zhu X-H, Kim SG, Georgopoulos G. Functional mapping in the human brain using high magnetic fields. *Philos Trans R Soc Lond B* 1999;354:1195–1213.
- Pan JW, Vaughan JT, Kuzniecky RI, Pohost GM, Hetherington HP. High resolution neuroimaging at 4.1T. *Magn Reson Imaging* 1995;13:915–921.
- Hetherington H, Kuzniecky R, Pan J, Mason G, Morawetz R, Harris C, Faught E, Vaughan T, Pohost G. Proton nuclear magnetic resonance spectroscopic imaging of human temporal lobe epilepsy at 4.1 T. *Ann Neurol* 1995;38:396–404.
- Hetherington HP, Luney DJ, Vaughan JT, Pan JW, Ponder SL, Tschendel O, Twieg DB, Pohost GM. 3D 31P spectroscopic imaging of the human heart at 4.1 T. *Magn Reson Med* 1995;33:427–431.
- Gruetter R, Garwood M, Ugurbil K, Seaquist ER. Observation of resolved glucose signals in 1H NMR spectra of the human brain at 4 Tesla. *Magn Reson Med* 1996;36:1–6.
- Gruetter R, Seaquist ER, Kim SG, Ugurbil K. Localized in vivo 13C NMR of glutamate metabolism in the human brain. Initial results at 4 Tesla. *Dev Neurosci* 1998;20:380–388.
- Pfeuffer J, Tkac I, Choi IY, Merkle H, Ugurbil K, Garwood M, Gruetter R. Localized in vivo 1H NMR detection of neurotransmitter labeling in rat brain during infusion of [1-13C] D-glucose. *Magn Reson Med* 1999;41:1077–1083.
- Gruetter R, Weisdorf SA, Rajanayagan V, Terpstra M, Merkle H, Truwit CL, Garwood M, Nyberg SL, Ugurbil K. Resolution improvements in in vivo 1H NMR spectra with increased magnetic field strength. *J Magn Reson* 1998;135:260–264.
- Lee S-P, Silva AC, Ugurbil K, Kim S-G. Diffusion weighted spin echo fMRI at 9.4 T: microvascular/tissue contribution to BOLD signal changes. *Magn Reson Med* 1999;42:919–928.
- Kim D-S, Duong T, Kim S-G. High-resolution mapping of iso-orientation columns by fMRI. *Nat Neurosci* 2000;3:164–169.
- Vaughan JT, Garwood M, Merkle H, Adriany G, Uckun FM, Ugurbil K. First 9.4T homogeneous head imaging of a monkey. In: *Proc 82nd Meeting RSNA*, 1996.
- Robitaille PM, Abduljalil AM, Kangarlu A, Zhang X, Yu Y, Burgess R, Bair S, Noa P, Yang L, Zhu H, Palmer B, Jiang Z, Chakeres DM, Spigos D. Human magnetic resonance imaging at 8 T. *NMR Biomed* 1998;11:263–265.
- Kangarlu A, Abduljalil AM, Robitaille PM. T1- and T2-weighted imaging at 8 Tesla. *J Comput Assist Tomogr* 1999;23:875–878.
- Vaughan JT, Garwood M, Collins CM, DelaBarre L, Adriany G, Andersen P, Merkle H, Smith MB, Ugurbil K. 7T vs. 4T: preliminary B1, SNR, SAR comparison in the human head. In: *Proc 8th Annual Meeting ISMRM*, Denver, 2000. p 147.
- Vaughan JT, Hetherington HP, Otu JO, Pan JW, Pohost GM. High frequency volume coils for clinical nuclear magnetic resonance imaging and spectroscopy. *Magn Reson Med* 1994;32:206–218.
- Vaughan JT. High frequency volume coils for nuclear magnetic resonance applications. US Patent 5,557,247; 1996.
- Zhang N, Roos M, Vaughan JT, Budinger T. Head coil B1 field inhomogeneity and SNR performance at 8-10T. In: *Proc 4th Annual Meeting ISMRM*, New York, 1996. p 252.
- Röschmann P. Letter to the editor; comments on “human magnetic resonance imaging at 8T.” *NMR Biomed Lett* 1999;12:315–317.
- Kunz KS, Luebbers RJ. The finite difference time domain method for electromagnetics. Boca Raton, FL: CRC Press; 1993.
- Gabriel C. Compilation of the dielectric properties of body tissues at RF and microwave frequencies. Air Force materiel command, Brooks Air Force Base, Texas: AL/OE-TR-1996-0037; 1996.
- Collins CM, Li S, Smith MB. SAR and B<sub>1</sub> field distributions in a heterogeneous human head model within a birdcage coil. *Magn Reson Med* 1998;40:847–856.
- Hoult DI. The principle of reciprocity in signal strength calculations—a mathematical guide. *Concepts Magn Reson* 2000;4:173–187.
- Edelstein WA, Glover GH, Hardy CJ, Redington RW. The intrinsic signal-to-noise ratio in NMR imaging. *Magn Reson Med* 1986;3:604–618.
- Haase A. Snapshot FLASH MRI. Applications to T1, T2, and chemical shift-maging. *J Magn Reson* 1990;13:77–89.
- Tannús A, Garwood M. Reducing RF power requirements of multislice imaging using a single adiabatic frequency swept inversion pulse. In: *Proc 4th Annual Meeting ISMRM*, New York, 1996. p 362.
- Röschmann P. Radiofrequency penetration and absorption in the human body: limitations to high-field whole-body nuclear magnetic resonance imaging. *Med Phys* 1987;14:922–931.
- Barfuss H, Fischer H, Hentschel D, Ladebeck R, Oppelt A, Wittig R, Duerr W, Oppelt R. In vivo magnetic resonance imaging and spectroscopy of humans with a 4 T whole-body magnet. *NMR Biomed* 1990;3:31.